Single-Shot Diffraction Autofocusing: Distance Prediction via an Untrained Physics-Enhanced Network

Ju Tang, Ji Wu, Jiawei Zhang, Zhenbo Ren, Jianglei Di, *Member, IEEE*, and Jianlin Zhao, *Member, IEEE*

***Abstract*—Deep learning technology has shown excellent performances and successful applications in optical information processing. However, the long-time training, large amount of manually labeled data and generalization capability hinder the application of deep neural network (DNN) under supervised learning. The deep image prior (DIP) opinion promotes the development of untrained neural network, which can learn from one image. Here we propose a DIP-based strategy to nest the DNN into a physical model for finding the optimal solution in a univariate optimization problem. The untrained physics-enhanced network (UPN) is proposed to predict the diffraction distance via only one diffraction pattern of a known phase object. Simulation and experimental results show that the UPN can be used to predict the distance precisely and consistently with different targets, diffraction distances as well as phase ranges, while it only takes a little time for training. In addition, the trained UPN can generalize to the other targets as long as the actual diffraction process keeps the same. Compared with the autofocusing metrics of holographic reconstruction and traversal method, the UPN has advantages in speed and accuracy, and it also has good noise resistance, which are all meaningful for the autofocusing of holographic reconstruction and imaging.**

***Index Terms*—Deep image prior, prediction of diffraction distance, physical model, untrained physics-enhanced network.**

I. Introduction

RECENTLY, deep learning technology has attracted a lot of attention because of its excellent performances in digital holography [1], [2], super-resolution imaging [3], scattering medium imaging [4], denoising [5], wavefront sensing [6], autofocusing [7], multi-wavelength interference [8] and image restoration [9], [10], etc. However, the deep neural network (DNN) almost needs long-time training with a dataset yet, which contains a large number of inputs and labels [11], [12]. In many applications, such as measuring unknown phases, recovering clear images and identifying objects, acquiring large amounts of data requires high costs, and labeling these data is a combination of difficulties and costs. In addition, the supervised learning way also brings new requirements in driving parameter optimization. The accurate corresponding label is not only the key to the actual performance of network, but also the hardest part to obtain in numerous optical inverse problems. At the same time, due to the noise, environmental disturbance and other factors, it is difficult to get a fine generalization effect on the actual physical process with pre-trained DNN model under the limited size of dataset, let alone transfer the DNN trained in simulation to the application in practice [13].

In fact, a large training dataset is the critic for generalization capability, rather than extracting feature ability. The designed structure of DNN provides the ability of capturing low-level image prior information in deep image prior (DIP) [14]. It's possible for DNN to learn from one image without any pre-trained models. Inspired by the DIP opinion, the untrained neural network is proposed for learning from one image under the physical constraint [15], and has been successfully applied to phase imaging, holographic reconstruction, diffraction tomography, computational ghost imaging and photography [16]–[19]. With the help of physical forward model, the untrained network can complete the optimization with one image or a few images in a short time, but has no generalization capability for object diversity, due to the information relevance between the object and output of network. It seems that the problems of long-time training, large amount of data, and accurate labels are all solved effectively at the expense of generalization capability. However, the precise physical forward model is the key to add more physical constraints in an untrained network, and may have discrepancy with the actual process easily due to the imprecision of some parameters or processes, leading to a rapid decline in effectiveness.

A typical DNN-based approach requires numerous parameters to fit the forward physical model or inverse solution relationship through a large amount of data [4], [6]. That is clumsy and time-consuming because some phenomena could

Manuscript received November 29, 2021; revised December 15, 2021; accepted December 22, 2021. Date of publication December 28, 2021; date of current version January 4, 2022. This work was supported in part by the National Natural Science Foundation of China under Grants 62075183, 61927810, and 61905197, and in part by the Open Research Fund of State Key Laboratory of Transient Optics and Photonics under Grant SKLST202008. *(Corresponding author: Jianglei Di.)*

Ju Tang, Ji Wu, Jiawei Zhang, Zhenbo Ren, and Jianlin Zhao are with the Key Laboratory of Light Field Manipulation and Information Acquisition, Ministry of Industry and Information Technology and Shaanxi Key Laboratory of Optical Information Technology, School of Physical Science and Technology, Northwestern Polytechnical University, Xi'an 710129, China (e-mail: tangju@mail.nwpu.edu.cn; wuji@mail.nwpu.edu.cn; zhangjiawei@mail.nwpu.edu.cn; zbren@nwpu.edu.cn; jlzhao@nwpu.edu.cn).

Jianglei Di is with the Guangdong Provincial Key Laboratory of Photonics Information Technology, Guangdong University of Technology, Guangzhou 510006, China, and also with the Key Laboratory of Light Field Manipulation and Information Acquisition, Ministry of Industry and Information Technology and Shaanxi Key Laboratory of Optical Information Technology, School of Physical Science and Technology, Northwestern Polytechnical University, Xi'an 710129, China (e-mail: jiangleidi@gdut.edu.cn).

Digital Object Identifier 10.1109/JPHOT.2021.3138548

This work is licensed under a Creative Commons Attribution-NonCommercial-NoDerivatives 4.0 License. For more information, see https://creativecommons.org/licenses/by-nc-nd/4.0/

be precisely simulated and analyzed in optics, while the DNN must refit these processes at the risk of mismatching the physical reality. The untrained network enables tighter integration of the network model with physical constraints, but an accurate physical model is not easily available. In fact, many optical processes can be approximated in computational optical imaging, but the difficulty of accurate model almost lies in some hard-to-measure parameters. Can these parameters be incorporated into the optimization space of neural network for direct solution? In this paper, a DIP-based idea is put forward: nesting the network into a physical model, where the network is used to fit some hard-to-model processes or difficult-to-measure parameters.

Autofocusing for holography and imaging is a significant research problem, and has significant results achieved by combining with deep neural network in recent years [20], [21]. However, traditional autofocusing criteria, such as Contrast, L1-norm Gradient, Laplacian of Gaussian, Tenenbaum Gradient and Variance [22], [23], are all susceptible to misjudgment due to the noise and complex samples. The deep learning-based autofocusing methods, whether predicting reconstruction distances [24], [25], or generating focused images directly [26], are still suffering from the above drawbacks associated with supervised learning. In fact, the prediction of reconstruction distance is equal to that of diffraction distance in monochromatic coherent light. For the preliminary verification of DIP-based idea, here we choose the prediction of diffraction distance problem as the example, and propose an untrained physics-enhanced network (UPN) to predict distance via only one diffraction pattern of the known phase. At first, the diffraction and network model are introduced to form UPN. In simulation and experiment, the UPN can predict the diffraction distance precisely with different objects, diffraction distances, and phase ranges. The training of UPN takes a small amount of time (<30 s for 256 × 256 pixels) due to the significant reduction in numbers of network parameters and training data. In addition, the trained UPN can generalize to the other objects if the actual diffraction process keeps the same. Compared with the autofocusing metrics of holographic reconstruction and traversal method, the UPN has advantages in speed and accuracy. In discussion, the optimization under noises in simulation and experiment are compared for verifying the noise resistance. Furthermore, the strategy may be easily extended to other imaging problems.

II. Theory and Method

A. Diffraction Model

Diffraction is a common optical phenomenon, and predicting the diffraction distance is significant for holographic reconstruction and imaging [20], [21], [24]–[26]. According to the angular spectrum theory, the diffraction process can be simulated accurately and calculated quickly in mathematics. Therefore, the computational diffraction model can be combined with the neural network model to add a strict physical constraint in UPN, and the pipeline of UPN is shown in Fig. 1(b). Here we use the diffraction of phase object as an example, and UPN is also applied to the amplitude target. From Fig. 1(b), the

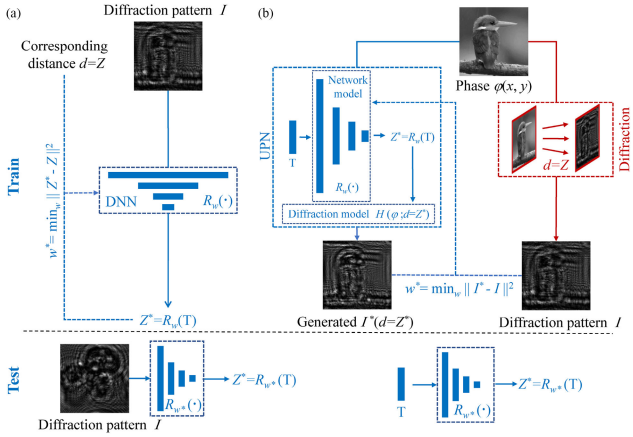

Fig. 1. Schematic illustration of DNN and UPN in prediction of diffraction distance. (a) Diffraction pattern I is taken into DNN under the supervision of corresponding distance $d = Z$. Another diffraction pattern is used for testing the generalization capability of trained DNN. (b) A measured diffraction pattern I of the phase object φ is obtained through $d = Z$ diffraction with 35 dB uniform noise. The network $R_w(\cdot)$ is taken to produce the distance Z^* from a fixed array T. Then the known phase φ is numerically propagated to get the generated pattern I^* through $H(\varphi; d = Z^*)$. The mean square error (MSE) between I and I^* is taken as loss value to adjust parameters w. After training, the distance Z^* is generated from the fixed array T, no matter what the object is.

measured diffraction pattern I of phase object is obtained with the diffraction to a distance Z and ∼35 dB uniform noise. The network model is taken to produce the predicted distance Z^* from a fixed array T. Then the known phase φ is numerically propagated to get generated pattern I^* through the calculation diffraction model. The mean square error (MSE) between I and I^* is calculated as the loss function to adjust weights and biases of network model. The UPN can learn to predict the diffraction distance quickly only using the phase and corresponding diffraction pattern, without the needs for long-time training and large amounts of labeled data. It is obvious that the network model is not connected to either the phase object or the diffraction pattern. As long as the actual diffraction process keeps the same, the UPN always gives the accurate prediction no matter how objects change.

Specifically, for a phase object $\varphi(x, y)$, according to the Fresnel diffraction theory, the complex amplitude under the illumination of a coherent plane wave can be written as

$$U_0(x, y; d = 0) = \exp[i\varphi(x, y)], \tag{1}$$

$$\begin{aligned} G_d(f_x, f_y) &= G_0(f_x, f_y) \cdot A(f_x, f_y) \\ &= G_0(f_x, f_y) \cdot \exp\left[ikZ\sqrt{1 - \lambda^2 f_x^2 - \lambda^2 f_y^2}\right]. \end{aligned} \tag{2}$$

Where, U_0 and U_d are the complex amplitude at the distance $d = 0$ and $d = Z$ from the object plane, G_0 and G_d are the Fourier transform of U_0 and U_d, A is the transfer function, and f_x and f_y are the spatial frequencies in the x and y directions, respectively. Then, the diffraction pattern at distance Z is expressed as

$$I(d = Z) = |U_d(x, y; d = Z)|^2 = H(\varphi; Z), \tag{3}$$

where $H(\varphi; Z)$ represents that the intensity diffraction pattern, I is the result of phase φ and distance Z through the mapping function $H(\cdot)$.

B. Untrained Physics-Enhanced Network

Through the inverse process $H^{-1}(\cdot)$ with constant phase, the distance prediction can be expressed as

$$Z = H^{-1}[I(d = Z)]. \tag{4}$$

From Fig. 1(a), the typical DNN-based method takes the diffraction patterns I_i and the distances d_i $(i = 1, 2, ..., N)$ as the inputs and labels, and then minimize the loss values between the network outputs and labels [27], [28]. The training and testing process can be formulated as

$$R_{w^*} = \text{argmin}_w ||R_w(I_i) - d_i||^2, \tag{5}$$

$$Z^* = R_{w^*}(I), \tag{6}$$

where w and w^* are the network weights before and after training, R_{w^*} is the optimal mapping function from the diffraction pattern to corresponding distance, Z^* is the predicted distance of network. In Fig. 1(a), the diffraction pattern I_i is taken as the input of network $R_w(\cdot)$, and the weights are optimized under the supervision of corresponding distance d_i to fit the relationship $H^{-1}(\cdot)$. However, the training always needs even tens of thousands image pairs as the dataset and takes several hours for optimization. It will inevitably lead to a decrease in the predicted effect, when only the diffraction pattern of one object is used to train DNN and that of another object is used for testing. And the range of distances within dataset limits the actual performance of DNN greatly, since the highly questionable generalization capability of supervised learning currently. As for UPN, the formula is changed as

$$Z^* = \text{argmin}_d ||H(\varphi; d = R_w(\mathrm{T})) - I(d = Z)||^2, \tag{7}$$

where T is just a fixed array, not directly related to the object and diffraction pattern.

From Fig. 1(b), we use the simulated process $H(\varphi; d = R_w(\mathrm{T}))$ to get the generated I^*, and calculate the MSE between I and I^* to optimize the parameters. This will force the generated I^* to converge to the diffraction pattern I through an iterative process, and at this time Z^* will converge to Z. That means that UPN can predict the distance with only one phase and corresponding diffraction pattern, instead of collecting lots of image pairs as the dataset. In fact, the network model optimizes the parameters according to the loss values and generates Z^* from T, independent of the specific distribution of diffraction pattern. As a result, the corresponding generated pattern I^* must conform to the physical constraints, and the UPN trained by target A can transfer to other targets as long as the actual diffraction process keeps the same. If the diffraction distance changes, the UPN needs to be retrained with a little time, due to the small amount of the data and parameters.

We design the network as only four blocks (fully connected layer + batch normalization layer + sigmoid) to output the predicted distance Z^* from T. The Array T is reshaped to 1000, 100, 10 numbers and output 1 number as Z^* through the network $R_w(\cdot)$. Here the prediction of distance is only a univariate optimization problem, so the network is really simple. The deeper network with more outputs can be used on multivariate optimization problems. The UPN is implemented based on the TensorFlow-1.9.0 platform using Python 3.6.13. The phase image φ and diffraction pattern I were reshaped to 256×256 pixels. The optimization usually needs 4000 steps to find a good solution within 30 s. The Adam optimizer with a learning rate of 0.1 is adopted to optimize the parameters. With the combination of large learning rate optimization and weight reinitialization, the optimization can be understood as a similar random search for the optimal solution interval at this time. Once the loss function is reduced significantly, the learning rate will gradually decrease to obtain a more accurate solution. All processed are dealt on a computer with an Intel Core i7-10700 K CPU, 32 GB of RAM, and an NVIDIA 1080Ti GPU.

As a result, the UPN has several advantages compared with the typical DNN: 1) One image pair is enough for training. This greatly reduces the cost and difficulty of data acquisition. 2) A small amount of training data and the simple network structure make the training time and computational cost lower significantly. 3) The network model is constrained by the diffraction model. As a part of UPN, the network model just contributes a key parameter to result. That makes the result of UPN adhere to the constraints of physical model strictly. 4) The trained UPN can generalize to any targets as long as the diffraction process remains the same, due to the fact that the network model is not directly connected to the target information. In order to fully verify the above advantages, simulated and experimental data are brought to analysis as follows.

III. Results and Discussions

A. Simulation for the Diversity and Stability of Objects, Distances and Phases

We choose 20 images as the phase targets to verify the actual performance of UPN in simulation. The results of target A, B, C and D are shown in Fig. 2 for the comparisons with various targets, diffraction distances and phase ranges, assuming that the diffraction distance is limited to [0, 100] mm. The target A and B with a phase of 2π propagate to 15.600 mm and 42.800 mm in Fig. 2(a), and the target C and D with a phase of 4π propagate to 67.200 mm and 89.100 mm in Fig. 2(c), respectively. After the fast training with one phase and corresponding diffraction pattern I, the UPN can give the predicted distance Z^* and then generated I^*. The generated patterns I^* are nearly identical to the diffraction patterns I, and the absolute errors between Z and Z^* are all less than 0.1 mm on four targets. We repeat the prediction of Fig. 2(a) 50 times in Fig. 2(b) to avoid the accidental results, and the average values are shown in Table I. The predicted distances of UPN are generally stable, and the mean absolute errors (MAE) of target A and B are only 0.003 mm and 0.012 mm, respectively. As for the influence of phase range, we repeat the prediction of Fig. 2(c) 30 times with different maximum phases in Fig. 2(d). The distribution of predicted distances is relatively concentrated and stable, and their MAE of target C and D in Table I is 0.048 mm and 0.014 mm, respectively.

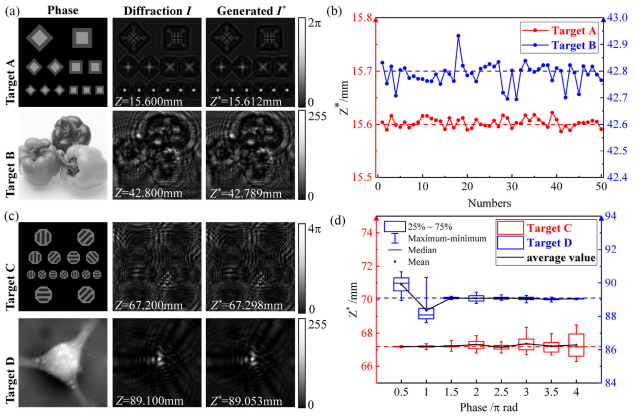

Fig. 2. Prediction of diffraction distance via UPN in simulation. (a) Results of Target A and B with 2π rad phase and their diffraction patterns at 15.600 mm and 42.800 mm, respectively. (b) Repeating the prediction 50 times of (a). (c) Results of Target C and D with 4π rad phase and their diffraction patterns at 67.200 mm and 89.100 mm, respectively. (d) Repeating the prediction 30 times of (c) with the changing phase ranges.

TABLE I
AVERAGE VALUES OF PREDICTION IN FIG. 2

	Target A	Target B	Target C	Target D
Average time /s	8.899	28.849	25.552	26.649
Average Z^* /mm	15.603	42.788	67.248	89.096
MAE /mm	0.003	0.012	0.048	0.014

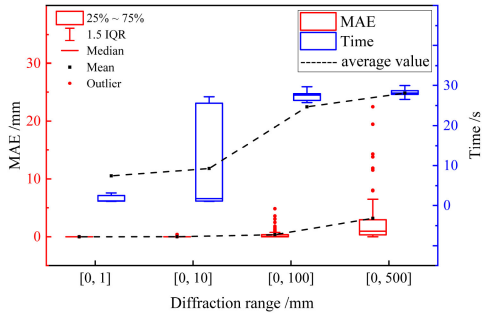

Fig. 3. Repeating the prediction 100 times in different diffraction ranges. The phase targets, phase ranges and diffraction distances (Z) are all randomly selected.

So it seems that the UPN can predict the diffraction distance accurately with various targets, diffraction distances and phase ranges.

To further demonstrate the stability of predictions, we consider four diffraction ranges: [0, 1], [0, 10], [0, 100] and [0, 500] mm. All targets are chosen randomly to generate diffraction patterns with random phases in [0, 4π] and random diffraction distances in above four ranges. The actual distribution and specific average values of 100 times prediction are all shown in Fig. 3 and Table II. The predictions are relatively accurate and stable in all diffraction ranges except [0, 500] mm. The MAE and average time increase as the diffraction range becomes larger, while the outlier values also become more outrageous. We define the absolute error within 1% of the diffraction range as the accurate value, and the accuracy rates of four ranges are listed in Table II. The accuracy rates are also falling with the increasing of diffraction range, which is constant with the changes in MAE. As the diffraction distance increases, the high-frequency information in the diffraction pattern has been gradually lost, leading to the difficulty for the network model to learn from Fig. 2(a) and (c). About the time cost, UPN always completes the one prediction within 30 s from Tables I and II.

TABLE II
AVERAGE VALUES OF 100 TIMES PREDICTION IN FIG. 3

Diffraction range /mm	[0, 1]	[0, 10]	[0, 100]	[0, 500]
Average time /s	7.435	9.278	24.672	28.080
MAE /mm	0.003	0.012	0.358	3.180
Accuracy	100%	98%	90%	89%

B. *Experiment for the Prediction of Diffraction Distances*

The experimental setup is shown in Fig. 4(a). The light can be regarded as a plane wave after beam expansion and collimation, and then it is incident on the spatial light modulator (SLM, CAS MICROSTAR FSLM-2k55-P) after modulation by a polarizer. The wavelength is 532 nm, and the SLM produces a phase modulation of [0, 2π] by loading the phase targets. The reflected light enters the camera for imaging through a non-polarizing beam splitter (NPBS). The diffraction distance Z is from the SLM target surface to the camera target surface, which is difficult to obtain precisely in experimental. We choose target E and F to propagate to the same distance ($\sim$50 mm), and thus get the phases and diffraction patterns I for UPN. Subsequently, we record the corresponding holograms by adding the reflector and polarizer in the dashed box of Fig. 4(a) to form the reference beam, which can interfere with the diffraction beam. The autofocusing metrics of holographic reconstruction, including the Contrast, L1-norm Gradient (LG), Laplacian of Gaussian (LOG), Tenenbaum Gradient (TG) and Variance, are all used to perform the automatic determination of distance [27-29], and the generated patterns obtained at the corresponding distances are taken for comparison with UPN in Fig. 4(b). The UPN predicts the distances as 46.136 mm and 46.431 mm from targets E and F, while the predicted distances by autofocusing metrics have a huge difference. As the most stable one of metrics, the LOG metrics predict 48.442 mm and 47.236 mm, and the absolute error is 1.206 mm according to the same diffraction process with different targets. However, the absolute error of UPN is just 0.295 mm, which is much lower than those of metrics, and still consistent with the results of simulation. All generated patterns are all taken for comparison with the diffraction pattern I by root mean square error (RMSE), peak signal-to-noise ratio (PSNR) and structural similarity (SSIM) in Table III. The generated pattern at the distance predicted by UPN is the most similar to the diffraction pattern by these image indexes, which means that UPN predicts the most accurate diffraction distance. In general, the autofocusing metrics are susceptible to the irregular samples and noises, while the UPN is more stable. The UPN with the

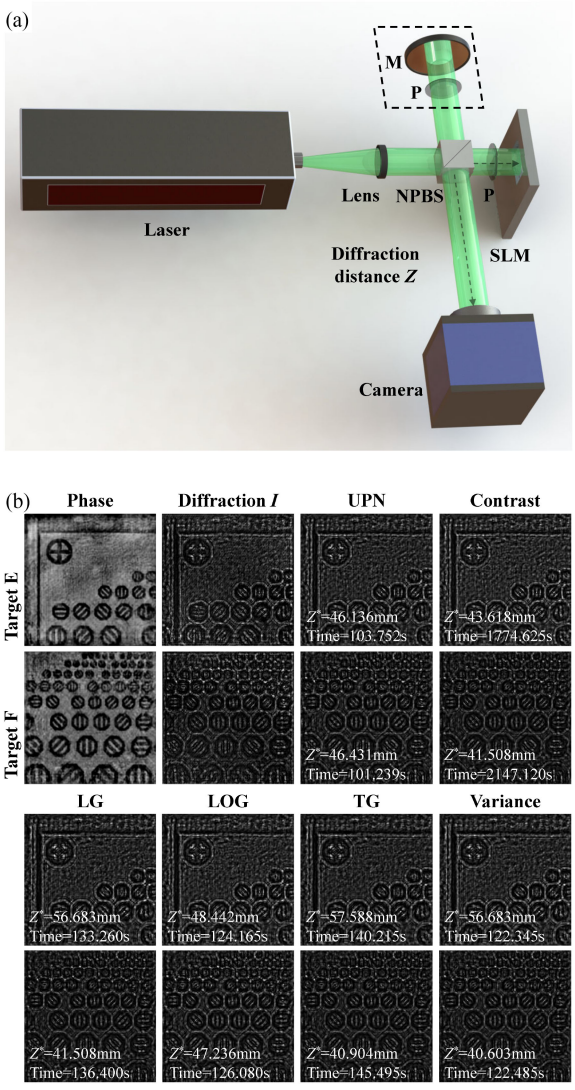

Fig. 4. (a) Experimental setup. NPBS: non-polarizing beam splitter. SLM: spatial light modulator. P: polarizer. M: mirror. (b) Prediction of diffraction distance via UPN in experiment. Target E and F both captured at the same diffraction distance. All autofocusing metrics are used for searching the diffraction distance from the corresponding hologram.

TABLE III
IMAGE INDEXES BETWEEN GENERATED PATTERNS AND DIFFRACTION PATTERNS IN FIG. 4

	Index	UPN	Contrast	LG	LOG	TG	Variance
Target E	RMSE	**16.040**	17.160	19.813	16.140	19.977	19.813
	PSNR /dB	**24.027**	23.440	22.192	23.973	22.120	22.192
	SSIM	**0.801**	0.777	0.668	0.798	0.648	0.668
Target F	RMSE	**16.905**	17.819	17.819	17.030	18.026	18.131
	PSNR /dB	**23.570**	23.113	23.113	23.507	23.013	22.963
	SSIM	**0.766**	0.723	0.723	0.767	0.714	0.710

1024 × 1024 pixels target takes ∼100 s for searching within [0, 100] mm in experiment, while all autofocusing metrics takes 120 s at least for searching from 40 mm to 60 mm with 200 steps. Eventually, the UPN can produce the stable and precise prediction with the least time in experiment.

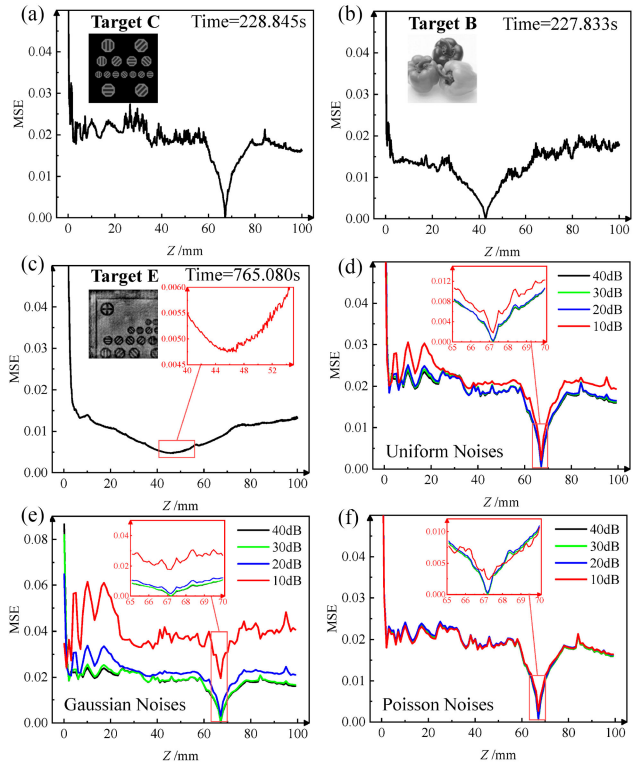

Fig. 5. Curve of MSE with 0–100 mm diffraction. Three phase targets with 2π rad phase, and the MSE between diffraction pattern I and generated I^* is calculated. (a) and (b) Target C and B with 256 × 256 pixels propagate to 67.200 mm and 42.800 mm without additional noises in simulation, respectively. (c) Target E with 1024 × 1024 pixels propagates to 46 mm in experiment. (d)–(f) Target C with 256 × 256 pixels propagates to 67.200 mm with 40 dB, 30 dB, 20 dB and 10 dB Uniform, Gaussian and Poisson noises in simulation, respectively.

C. Discussions About Optimization Under Noises

Now we focus on the optimization process of network models in simulation and experiment, and the curves of MSE are shown in Fig. 5. Three phase targets with 2π rad are taken for comparison, and the MSE between diffraction pattern I and generated I^* is calculated. The curves of targets B and C have distinct minimum values at the corresponding diffraction distances without noises in simulation, while that of target E is vague in experiment. Under the influence of noises and experimental errors, the MSE of target E is difficult to converge to as low as that in the simulation, which may lead to more difficulties in optimizing the network model. However, it can be seen from the enlargement curve that the lowest point still exists and is very close to the prediction in Fig. 4(b), indicating that UPN is able to find the most suitable distance accurately in experiment. When the traversal range is [0, 100] mm with 0.1 mm intervals, the traversal searching of targets B, C and E take 227.833 s, 228.845 s and 765.080 s, while UPN takes 28.849 s, 25.525 s and 103.752 s, respectively. It is obvious that the UPN has advantages over the traversal method for the univariate optimization problems.

As for the influence of the noise type and level, Fig. 5(e)–(f) are taken for comparison. The Uniform, Gaussian and Poisson noises with 40 dB, 30 dB, 20 dB and 10 dB signal-to-noise ratio

(SNR) are added into the Target C in Fig. 5(a). From Fig. 5(e)–(f), all curves still have obvious lowest points, indicating that the optimal solution exists. In contrast, the lowest point with 10 dB Gaussian noise is not obvious in magnified view, and the curve trend is also different from others. As a result, the UPN has ~ 2 mm prediction error under Gaussian noise while <0.14 mm under others with 10 dB SNR. With 40 dB, 30 dB and 20 dB SNR, the UPN keeps the errors within 0.07 mm under three types noises. It can be seen that the UPN has good resistance for optimizing to the optimal solution under noises.

Although the UPN has high accuracy, generalization capability to other objects and noise resistance, it still has some existing problems for further researching. The DIP-based idea is verified in a univariate optimization problem, so the phase of object is taken as a known parameter, which causes the problems of application in autofocusing. The multivariate optimization and the application in autofocusing with unknown objects are taken into consideration in process.

IV. Conclusion

In this paper, we have presented a DIP-based idea to nest DNN with the physical model, and chosen a univariate optimization problem to verify the feasibility. The untrained physics-enhanced network (UPN), which containing the network model and the diffraction model, is proposed to predict the diffraction distance via only one diffraction pattern of a known phase. The simulation and experiment show that the UPN can be used to predict the distance precisely and consistently with various targets, diffraction distances and phase ranges. And it has advantages over the autofocusing metrics of holographic reconstruction and traversal method in speed and accuracy. The influence of noises is discussed by comparing the optimization process and prediction errors. However, the prediction of diffraction distance is just a simple univariate optimization problem, and our DIP-based idea needs further verified. In future work, we will extend to multivariate optimization problems to integrate DNN with physical processes more closely, and make full use of the advantages of DNN in practice.

References

[1] K. Wang, Y. Li, Q. Kemao, J. Di, and J. Zhao, "One-step robust deep learning phase unwrapping," *Opt. Exp.*, vol. 27, no. 10, pp. 15100–15115, 2019.

[2] J. Wu, K. Liu, X. Sui, and L. Cao, "High-speed computer-generated holography using an autoencoder-based deep neural network," *Opt. Lett.*, vol. 46, no. 12, pp. 2908–2911, 2021.

[3] Y. Gao and L. Cao, "Generalized optimization framework for pixel super-resolution imaging in digital holography," *Opt. Exp.*, vol. 29, no. 18, pp. 28805–28823, 2021.

[4] M. Lyu, H. Wang, G. Li, S. Zheng, and G. Situ, "Learning-based lensless imaging through optically thick scattering media," *Adv. Photon.*, vol. 1, no. 3, 2019, Art. no. 036002.

[5] K. Yan, Y. Yu, T. Sun, A. Asundi, and Q. Kemao, "Wrapped phase denoising using convolutional neural networks," *Opt. Lasers Eng.*, vol. 128, 2020, Art. no. 105999.

[6] K. Wang *et al.*, "Deep learning wavefront sensing and aberration correction in atmospheric turbulence," *PhotoniX*, vol. 2, no. 1, pp. 1–11, 2021.

[7] H. Ding *et al.*, "Auto-focusing and quantitative phase imaging using deep learning for the incoherent illumination microscopy system," *Opt. Exp.*, vol. 29, no. 17, pp. 26385–26403, 2021.

[8] J. Li, Q. Zhang, L. Zhong, and X. Lu, "Hybrid-net: A two-to-one deep learning framework for three-wavelength phase-shifting interferometry," *Opt. Exp.*, vol. 29, no. 21, pp. 34656–34670, 2021.

[9] J. Tang *et al.*, "Restorenet: A deep learning framework for image restoration in optical synthetic aperture imaging system," *Opt. Lasers Eng.*, vol. 139, 2021, Art. no. 106463.

[10] J. Tang *et al.*, "Restorenet-plus: Image restoration via deep learning in optical synthetic aperture imaging system," *Opt. Lasers Eng.*, vol. 146, 2021, Art. no. 106707.

[11] Y. Li, Y. Xue, and L. Tian, "Deep speckle correlation: A deep learning approach toward scalable imaging through scattering media," *Optica*, vol. 5, no. 10, pp. 1181–1190, 2018.

[12] I. Goodfellow, Y. Bengio, and A. Courville, *Deep Learning*. Cambridge, MA, USA: MIT press, 2016.

[13] X. Zhang, Q. Chen, R. Ng, and V. Koltun, "Zoom to learn, learn to zoom," in *Proc. IEEE/CVF Conf. Comput. Vis. Pattern Recognit.*, 2019, pp. 3762–3770.

[14] D. Ulyanov, A. Vedaldi, and V. Lempitsky, "Deep image prior," in *Proc. IEEE Conf. Comput. Vis. Pattern Recognit.*, 2018, pp. 9446–9454.

[15] F. Wang *et al.*, "Phase imaging with an untrained neural network," *Light: Sci. Appl.*, vol. 9, no. 1, pp. 1–7, 2020.

[16] E. Bostan, R. Heckel, M. Chen, M. Kellman, and L. Waller, "Deep phase decoder: Self-calibrating phase microscopy with an untrained deep neural network," *Optica*, vol. 7, no. 6, pp. 559–562, 2020.

[17] K. C. Zhou and R. Horstmeyer, "Diffraction tomography with a deep image prior," *Opt. Exp.*, vol. 28, no. 9, pp. 12872–12896, 2020.

[18] S. Liu, X. Meng, Y. Yin, H. Wu, and W. Jiang, "Computational ghost imaging based on an untrained neural network," *Opt. Lasers Eng.*, vol. 147, 2021, Art. no. 106744.

[19] K. Monakhova, V. Tran, G. Kuo, and L. Waller, "Untrained networks for compressive lensless photography," *Opt. Exp.*, vol. 29, no. 13, pp. 20913–20929, 2021.

[20] L. Silvestri *et al.*, "Universal autofocus for quantitative volumetric microscopy of whole mouse brains," *Nature Methods*, vol. 18, no. 8, pp. 953–958, 2021.

[21] Y. Wu *et al.*, "Three-dimensional virtual refocusing of fluorescence microscopy images using deep learning," *Nature Methods*, vol. 16, no. 12, pp. 1323–1331, 2019.

[22] Z. Ren, E. Y. Lam, and J. Zhao, "Acceleration of autofocusing with improved edge extraction using structure tensor and schatten norm," *Opt. Exp.*, vol. 28, no. 10, pp. 14712–14728, 2020.

[23] Y. Zhang, H. Wang, Y. Wu, M. Tamamitsu, and A. Ozcan, "Edge sparsity criterion for robust holographic autofocusing," *Opt. Lett.*, vol. 42, no. 19, pp. 3824–3827, 2017.

[24] H. Pinkard, Z. Phillips, A. Babakhani, D. A. Fletcher, and L. Waller, "Deep learning for single-shot autofocus microscopy," *Optica*, vol. 6, no. 6, pp. 794–797, 2019.

[25] Z. Ren, Z. Xu, and E. Y. Lam, "Learning-based nonparametric autofocusing for digital holography," *Optica*, vol. 5, no. 4, pp. 337–344, 2018.

[26] Y. Luo, L. Huang, Y. Rivenson, and A. Ozcan, "Single-shot autofocusing of microscopy images using deep learning," *ACS Photon.*, vol. 8, no. 2, pp. 625–638, 2021.

[27] G. Barbastathis, A. Ozcan, and G. Situ, "On the use of deep learning for computational imaging," *Optica*, vol. 6, no. 8, pp. 921–943, 2019.

[28] Y. Xue, S. Cheng, Y. Li, and L. Tian, "Reliable deep-learning-based phase imaging with uncertainty quantification," *Optica*, vol. 6, no. 5, pp. 618–629, 2019.